ELSEVIER

www.elsevier.nl/locate/jorganchem

Journal of Organometallic Chemistry 593–594 (2000) 403–408

Journal of Organometallic Chemistry

Structural properties of the metallointercalator cationic complex (2,2′:6′,2″-terpyridine)methylplatinum(II) ion

Raffaello Romeo [a,*], Luigi Monsù Scolaro [a], Maria Rosaria Plutino [a], Alberto Albinati [b]

[a] *Dipartimento di Chimica Inorganica, Chimica Analitica e Chimica Fisica, Università di Messina and Istituto di Chimica e Tecnologia dei Prodotti Naturali (ICTPN-CNR), Sezione di Messina, Vill. S. Agata, Salita Sperone, 31, I-98166 Messina, Italy*

[b] *Istituto di Chimica Farmaceutica e Tossicologica, Università di Milano, Milan, Italy*

Received 13 July 1999; accepted 29 September 1999

Abstract

The complex $[Pt(tpy)(Me)]^+(BPh_4)^-$ (tpy = 2,2′:6′,2″-terpyridine) crystallizes in the triclinic space group $P\bar{1}$ with $a = 13.463(2)$ Å, $b = 13.618(3)$ Å, $c = 20.151(4)$ Å, $\alpha = 73.59(2)$, $\beta = 74.56(3)$, $\gamma = 65.82(2)°$ and $Z = 4$. The final conventional R factor is 0.035. In the unit cell a couple of weakly interacting dimers are formed by stack of two $[Pt(tpy)(Me)]^+$ cations in a head-to-tail fashion with intermolecular Pt···Pt distances of 4.437(1) and 4.931(1) Å, respectively. The absorption spectra of $[Pt(tpy)(Me)]^+(BPh_4)^-$ in acetonitrile show bands assigned to π–π* and to MLCT transitions. The analysis of the dependence of the spectra on complex concentration gives a fairly low value for the dimerization equilibrium constant ($K_d = 180 \pm 52$ M^{-1} at 298 K). These fluid solutions are not emissive. The room-temperature solid-state emission spectra of the salts [Pt(tpy)(Me)]X are strongly dependent on the counterion ($X = BPh_4^-$, Cl^-, PF_6^-, ClO_4^-, $CF_3SO_3^-$). The cationic complex shows a considerable stability upon acidification and carbonilation in water.

Keywords: Head-to-tail dimers; Acetonitrile; Stability

1. Introduction

Platinum(II) complexes containing terpyridine are extensively investigated because of their outstanding spectroscopic and chemical properties. They are well-suited to interact with proteins [1,2] or to intercalate into DNA [3], oligomerize in solution [3–5] and in the solid state [3,5–9] showing ligand–ligand and metal–metal interactions, are good emitters both as solids or in the fluid state [5,8–12]. The electronic and photophysical properties of the planar Pt(tpy) molecular fragment can be tuned through an appropriate choice of the fourth ligand or of substituents on the terpyridine moiety. In this context, some years ago we reported the synthesis and characterization of $[Pt(tpy)(Me)]^+$ (**1**), one of the few platinum(II) complexes of terpyridine containing a Pt–C bond [13,14]. We have used a number of physical methods, including resonance light scattering measurements, to study the self-aggregation of this compound in aqueous solution and its interaction with nucleic acids [13,15]. The aggregative phenomena with biological matrices are rather complicated involving the distribution of complex **1** between its free self-aggregated form in solution, a non-organized aggregation on the backbone of the polymeric template and, at low drug loads, intercalative interaction. Highly organized supramolecular assemblies are formed on α-helical poly(L-glutamic acid) [16]. Complex **1** is luminescent in a 4:1(v/v) MeOH–EtOH rigid matrix at 77 K, with an unstructured luminescent band at 730 nm ($\tau = 1$ μs) originating from metal–metal interactions of oligomerized species [17]. We were able to grow single crystals of the tetraphenylborate salt of complex **1** suitable for X-ray analysis and here we report its molecular structure and additional photochemical and chemical measurements to complete the picture of this organometallic terpyridine complex.

* Corresponding author. Tel.: +39-090-391984; fax: +39-090-393756.

E-mail address: raf.romeo@chem.unime.it (R. Romeo)

0022-328X/00/$ - see front matter
PII: S0022-328X(99)00580-X

1.1. Instrumentation

NMR spectra were measured on a Bruker AMX R-300 spectrometer. UV–vis electronic spectra were recorded on a Cary 219 or a Hewlett-Packard HP8452 diode array spectrophotometer. A Jasco FP-750 spectrofluorimeter equipped with a Hamamatsu R928 phototube was used to obtain luminescence spectra. Emission maxima are uncorrected for photomultiplier response.

1.2. Preparation of complexes

The complex *trans*-[PtCl(Me)(Me_2SO)$_2$] (**2**) was prepared according to Eaborn et al. [18] and was purified by several crystallizations from dichloromethane–diethyl ether mixtures. The tetraphenylborate salt [**1**](BPh_4) was prepared according to a published method [13], by reacting **2** with tpy in methanol and adding $NaBPh_4$ to precipitate the compound.

1.3. [Pt(tpy)(Me)](BPh_4)

Anal. Calc. for $C_{40}H_{34}BN_3Pt_1$: H, 4.49; C, 63.0; N, 5.51. Found: H, 4,56; C, 62.3; N, 5.54. ^{1}H-NMR (0.01 M in dmso-d_6): δ 8.88 ($^3J_{PtH} = 50.9$ Hz, H_1); 8.60 (H_4, H_7); 8.52 (H_8); 8.44 (H_3); 7.85 ($^4J_{PtH} = 20.0$ Hz, H_2); 7.17–6.77 (phenyl groups); 1.10 ($^2J_{PtH} = 74.0$ Hz, CH_3) [19].

The compounds [**1**]Cl (**3**), [**1**](PF_6) (**4**), [**1**](CF_3SO_3) (**5**) and [**1**](ClO_4) (**6**) were prepared as reported elsewhere [13,14].

Table 1
Crystal data and structure refinement for compound [**1**]BPh_4

Formula	$C_{40}H_{34}BN_3Pt$
Molecular weight	762.60
Data collected Temperature (K)	296
Crystal system	Triclinic
Space group	$P\bar{1}$
a (Å)	13.463(2)
b (Å)	13.618(3)
c (Å)	20.151(4)
α (°)	73.59(2)
β (°)	74.56(3)
γ (°)	65.82(2)
V (Å^3)	3184.9(11)
Z	4
$\rho_{calc.}$ (g cm^{-3})	1.590
μ (cm^{-1})	44.39
Radiation	Mo–K_α (graphite monochromated $\lambda = 0.71079$ Å)
Measured reflections	$\pm h$, $\pm k$, $+l$
θ range (°)	$3.0 < \theta < 25.0$
No. of independent data	11128
No. of observed reflections (n_o)	7414[$\|F_o\| > 4.0\sigma(\|F\|)$]
Transmission coefficients	0.5341–0.9987
No. of parameters refined (n_v)	819
R, R_w^2 (observations, reflections) [a,b]	0.0346, 0.0908
R, R_w^2 (all data)	0.0752, 0.1065
Goodness-of-fit	1.022

[a] $R = \Sigma(|F_o| - (1/k)F_c|)/\Sigma|F_o|$.

[b] $R_w^2 = [\Sigma\, w(F_o^2 - (1/k)F_c^2)^2/\Sigma\, w|F_o^2|^2]$; GOF: $[\Sigma\, w(F_o^2 - (1/k)F_c^2)^2/(n_o - n_v)]^{1/2}$.

1.4. X-ray data collection and structure refinement

Crystals of [Pt(tpy)(Me)]BPh_4 (**1**), suitable for X-ray diffraction study, were grown by slow evaporation of concentrated methanol solutions. A pale orange crystal of [**1**](BPh_4) was mounted on a CAD4 diffractometer that was used for the unit cell and space group determination and for data collection. Unit cell dimensions were obtained by least squares fit of the 2θ values of 25 high order reflections. Selected crystallographic and other relevant data are listed in Table 1 and in Table S1 in Section 3. Data were measured with variable scan speed to ensure constant statistical precision on the collected intensities. Three standard reflections were used to check the stability of the crystal and of the experimental conditions and measured every hour; no significant variation was detected. Data were corrected for Lorentz and polarization factors using the data reduction programs of the MOLEN crystallographic package [20]. An empirical absorption correction was also applied (azimuthal (Ψ) scans of three reflections having $\chi > 85°$) [21]. The standard deviations on intensities were calculated in terms of statistics alone, while those on F_o were calculated as shown in Table 1.

The structure was solved by direct and Fourier methods and refined by full matrix least squares, minimizing the function $[\Sigma\, w(F_o^2 - (1/k)F_c^2)^2]$. Anisotropic temperature factors were used for all atoms. The contribution of the hydrogen atoms, in their calculated position, was included in the refinement using a riding model ($U_H = 1.5 \times U$ (bonded atom) Å^2). No extinction correction was deemed necessary. The scattering factors used, corrected for the real and imaginary parts of the anomalous dispersion, were taken from the literature [22]. Upon convergence the final Fourier difference map showed no significant peaks. All calculations were carried out by using the PC version of the SHELX-97 programs [23].

2. Results and discussion

2.1. Crystal structure

An ORTEP view of compound **1** is given in Fig. 1, while selected bond distances and angles are listed in

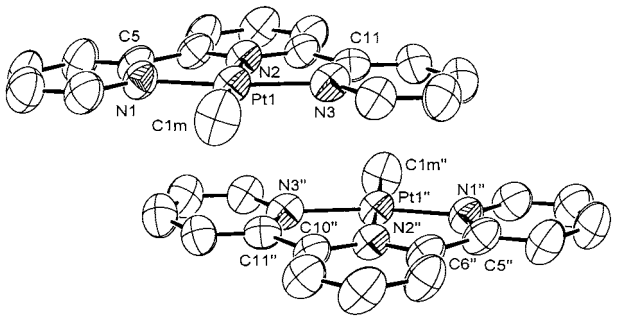

Fig. 1. ORTEP view of one of the two crystallographic independent molecules (Molecule 1). Thermal ellipsoids are drawn at the 50% probability level.

Table 2
Selected bond distances (Å) and angles (°) for the two crystallographically independent molecules [**1**]

	Molecule 1	Molecule 2
Bond distances		
Pt–N1	2.008(5)	2.016(5)
Pt–N2	1.976(4)	1.976(5)
Pt–N3	2.003(5)	2.014(5)
Pt–C1m	2.039(6)	2.054(7)
C5–C6	1.477(8)	1.480(9)
C10–C11	1.475(8)	1.467(9)
Bond angles		
N1–Pt–N3	160.8(2)	160.6(3)
N2–Pt–C1m	179.0(3)	176.8(3)
N1–Pt–N2	80.1(2)	80.2(3)
N1–Pt–C1m	99.6(3)	99.8(3)
N3–Pt–N2	80.7(2)	80.5(2)
N3–Pt–C1m	99.6(3)	99.6(3)

Table 2. The crystal structure consists of discrete, square planar $[Pt(tpy)(Me)]^+$ and $[BPh_4]^-$ units. There are two independent molecules in the unit cell (Fig. S1 in Section 3). Each cationic moiety interacts with another cationic unit (related by an inversion center) thus giving rise to a weakly interacting dimer in a head to tail arrangement. The best planes, calculated through the platinum atom, carbon atom and terpyridine ligand for these two adjacent units lie 3.42 Å apart. This distance is well within the value (3.8 Å) normally associated with a significant π–π interaction. The two independent dimeric units have different Pt···Pt separations, 4.437(1) and 4.931(1) Å, respectively. The overall packing is such that the two dimers related by symmetry are isolated from the other units by the surrounding tetraphenylborate anions. The coordination geometry in the two independent molecules in the unit cell is very similar: the differences in distances and angles being within the Estimated S.D.s. The only significant difference is that, in one of the two molecules, the square planar coordination presents a small tetrahedral distortion.

The immediate coordination sphere around the platinum contains the three nitrogens of the tpy ligand and the carbon of the methyl group. The Pt–C bond length (av. 2.047(9) Å) is in the range of values reported for a number of platinum(II) complexes [24]. The essential features of the tpy coordination sphere appear to be similar to those observed for other Pt(tpy) complexes, except for the Pt–N(2) bond distance (av. 1.976(4) Å) (the nitrogen in *trans* position to the strong σ-donor Pt–C bond). This is shorter than the bond to either of the other two nitrogens Pt–N(1) (av. 2.012(6) Å) and Pt–N(3) (av. 2.009(8) Å) but is significantly longer than the distances usually reported for the bond between platinum and the central nitrogen, because of the strong *trans*-influence of the opposite methyl group. The dimeric molecular structure of $[Pt(tpy)(Me)]^+$ is rather different from that of the analogous palladium compound [25], made up by discrete cations and anions, but shows strict similarities with the structure of the complex cation $[Pt(tpy)(CH_2NO_2)]^+$ [8], including the head-to-tail arrangement of the Pt_2 units (Pt–Pt = 3.4039(4) Å), the Pt–C bond distance of the carbon bonded nitromethyl group (2.076(6) Å) and the long Pt–N(2) bond distance (1.973(5) Å). A survey of the molecular structures of the [Pt(tpy)L]X complexes determined so far, indicates that the extent and the type of intermolecular interaction between the cationic moieties depend, among others, on the nature of the fourth ligand L and of the counteranion X. For example, the molecular structure of the salts $[Pt(tpy)(OMe)](BPh_4)$ [10] and $[Pt(tpy)(OH)](ClO_4)\cdot H_2O$ [26] is constituted by discrete cations and anions, while π–π stacking interactions between aromatic rings are dominating in the crystal packing of the salts $[Pt(tpy)(dpt)](ClO_4)$ [7] (dpt = 1,3-diphenyltriazine) and $[Pt(tpy)(mid)](ClO_4)_2$ [6] (mid = 1-methyl-imidazole) and, besides the two organometallic complexes discussed above, dimers stacking in a head-to-tail fashion are exhibited by the perchlorate [5] and the triflate [9] salts of $[Pt(tpy)Cl]^+$ (Pt–Pt distance = 3.269(1) and 3.329(1) Å, respectively).

2.2. Absorption spectroscopy

The complex [**1**](BPh_4) dissolves in acetonitrile to give pale yellow solutions. At low concentrations, the absorption spectrum (Fig. 2) shows well-resolved peaks at 408 nm ($\varepsilon = 2300\ M^{-1}\ cm^{-1}$), 337 (11950), 325 (10780), 313 (12780), and 270 (31150) which agree well with the data reported for the cationic complex in water [13] and in a 4:1 MeOH–EtOH mixture [17]. The maxima in the range of 310–340 nm are assigned to π–π* transitions of the coordinated tpy ligand and the band at 408 nm is assigned to a metal-to-ligand charge-transfer (CT) transition, in analogy to previous assignments for other [Pt(tpy)L]X complexes [5,9,10,17]. On increasing the concentration, the position of the peaks

remains almost unchanged but the absorption dependence on the complex concentration becomes non linear (see the inset in Fig. 2 for absorption data taken at 313 nm). The curvature in the Beer's law is interpreted as being due to aggregation of **1** in concentrated solutions. The linear region, at relatively low concentrations, is assumed to be due to the presence of monomeric $[Pt(tpy)(Me)]^+$ only. Using the value of $\varepsilon_M = 12780$ M^{-1} cm^{-1} calculated from the linear plot, we obtained values for the molar absorptivity of the dimer, $\varepsilon_D = 9100 \pm 612$ M^{-1} cm^{-1} at 313 nm and the constant for the equilibrium [D]/[M] [2], $K_d = 180 \pm 52$ M^{-1} at 298 K. The equation used for the curve fitting, derived from $A = \varepsilon_M[M] + \varepsilon_D[D]$ and $[D] = ([Pt]_0 - [M])/2$ is

$$A_M - A = ((2\varepsilon_M - \varepsilon_D)(4K_d[Pt]_0 + 1 - \sqrt{1 + 8K_d[Pt]_0}))/8K_d \quad (1)$$

where $[Pt]_0$ is the total concentration of complex and $A_M = \varepsilon_M[Pt]_0$.

The extent of aggregation of **1** in acetonitrile is by far less than that found in water ($K_d = 10 \times 10^3$ M^{-1}, from UV-vis experiments) [13]. The lower dielectric constant of the former disfavors the formation of a dicationic dimer. A similar effect has been observed by Gray et al. [4] on comparing the extent of the aggregation of $[Pt(tpy)Cl]^+$ in dimethylformamide and water. Evidence for extensive aggregation in water of **1** came also from the dependence of the ^{1}H-NMR spectra on complex concentration ($K_d = 26 \times 10^3$ M^{-1}, from ^{1}H-NMR experiments), comparable to that reported by Lippard [3b] for $[Pt(tpy)(SCH_2CH_2OH)]^+$ ($K_d = 6 \times 10^3$ M^{-1}). The observation of a large chemical shift change, especially for the methyl resonance, suggested that the structure in solution is like that in Fig. 1, with a parallel disposition of two planar units driven by π-stacking interactions between the aromatic moieties of the terpyridine ligand.

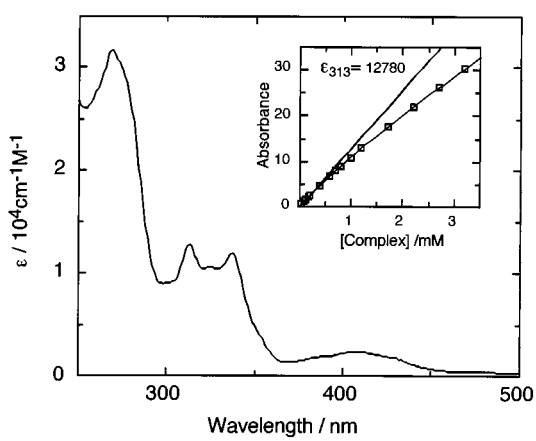

Fig. 2. Electronic spectrum of [**1**](BPh_4) in acetonitrile. In the inset: Beer's law experiments in acetonitrile. The line marked $\varepsilon_{313} = 12\,780$ defines Beer's law behavior for [**1**](BPh_4). The empty squares represent the experimental data and the line passing through the points is the theoretical curve obtained for the dimerization model with $\varepsilon_D = 9100 \pm 612$ M^{-1} cm^{-1} at 313 nm and $K_d = 180 \pm 52$ M^{-1} at 298 K.

2.3. Fluid and solid-state emission spectroscopy

Solutions of [**1**]X (X = BPh_4^-, Cl^-, PF_6^-, $CF_3SO_3^-$, ClO_4^-) complexes in degassed acetonitrile at room temperature exhibit a barely detectable emission band at 650 nm. Thus, $[Pt(tpy)(Me)]^+$, like the parent monocationic $[Pt(tpy)Cl]^+$ [9,12] and $[Pt(tpy)(X)]^{n+}$ (X = Br, I, N_3, NH_3) complexes, shows no significant photoluminescence intensity at room temperature in acetonitrile. This stands in contrast with the photoluminescence observed in fluid solution for $[Pt(tpy)(X)]^+$ (X = NCS, OMe, OH) [10] or for the $[Pt(4'\text{-R-tpy})Cl]^+$ series [9]. In some cases the lack of emission was attributed to the probable presence of low-lying d–d excited states, which can be easily populated by thermal activation, providing efficient deactivation pathways via molecular distortion [10,27].

The color of the solid samples of [**1**]X changes with the nature of the counter-ion X, being pale yellow for the hexafluorophosphate, triflate and perchlorate salts, whereas the chloride and the tetraphenylborate are orange. This in line with a number of reports indicating that the solid-state properties of the [Pt(tpy)L]X salts are strongly dependent on the nature of the ligand L, on the counter-ion, the solvent and the synthetic pathway. In particular, the range of colors of the [Pt(tpy)Cl]X salts seems to be due to the extent of metal–metal separation, and to the degree of oligomerization in the solid state [5]. Bailey et al. [5] examined the low-temperature solid-state luminescence of salts containing the $[Pt(tpy)Cl]^+$ moiety and concluded that the emission energy varied with the counterion (Cl^-, PF_6^-, $CF_3SO_3^-$, ClO_4^-). Likewise, microcrystalline samples of [**1**]X salts are emissive and their solid-state luminescence data at 300 K are reported in Table 3. Both the chloride and the hexafluorophosphate salts evidence a strong intensity, broad and structureless emission band at wavelength longer than 600 nm. The triflate and the tetraphenylborate display a medium

Table 3
Uncorrected emission maxima for [**1**]X solids at 300 K

X^-	λ_{max} (nm)	Color of [**1**]X
Cl^-	650	Orange [a]
PF_6^-	640	Yellow [b]
$CF_3SO_3^-$	505	Yellow [b]
$B(C_6H_5)_4^-$	530	Orange [b]
ClO_4^-	660 [c]	Yellow [b]

[a] Precipitated from dichloromethane–ethyl ether.
[b] Precipitated from methanol.
[c] Very weak emission intensity.

intensity feature at about 520 nm. On the contrary, the emission band of the perchlorate salt is rather weak, broad and centered at 660 nm. The interpretation of these data is not straightforward. It has been reported that the shape and the position of the emission peak are significantly related to the Pt–Pt distance, to the extent of π–π stacking between the aromatic moieties and to the nature of the counter-ion [5,9,11,27]. According to this view the emission data for the pair chloride–hexafluorophosphate would suggest a similar structure in the solid state as for the pair triflate–tetraphenylborate. For this last pair, the emission occurring at a significantly higher energy should arise from isolated monomers of [**1**]. This result is consistent with the rather long Pt–Pt distance found in the crystal packing of the tetraphenylborate salt. However, such a conclusion requires further verification since in platinum(II) terpyridine complexes, energy migration to defects or trap sites can affect the room temperature emission bands [28].

2.4. Chemical behavior in aqueous solution

Within the series of complexes examined, those having Cl^- and ClO_4^- as counterions are the most soluble in water. Spectrophotometric and NMR evidences indicate a cationic aggregation to form dimers in a head-to-tail conformation and oligomers, at the highest complex concentration [13]. These aqueous solutions are stable for weeks at room temperature. The chemical inertness of the $[Pt(tpy)(Me)]^+$ molecule towards hydrolysis and nucleophilic substitution is at the basis of its use as intercalator for nucleic acids. This inertness stands in contrast with the extreme lability of chloride in $[Pt(tpy)Cl]^+$ for which, kinetic studies of halide substitution in methanol, show rate enhancements of five to six order of magnitude with respect to the complex containing 1,5-diamino-3-azapentane (dien) as chelating ligand [29].

On adding hydrochloric acid 0.5 M to an aqueous solution of [**1**]Cl (2.0×10^{-4} M) the spectral changes observed in the UV-vis spectrum exhibit three isosbestic points and the final spectrum corresponds to that of [Pt(tpy)Cl]Cl. The process goes to completeness in about 20 min at 298 K. Thus, the Pt–C bond cleavage requires the addition of fairly high amounts of acid to occur in water. The plots of the absorbance, at selected wavelengths, against time have a sigmoidal shape. This phenomenon is associated to the presence of the dimer–monomer equilibrium in water. On decreasing the concentration of complex to 0.4×10^{-5} M not less than 90% of [**1**] is in the monomeric form, and the kinetics obey a first-order rate law until well over 90% conversion into [Pt(tpy)Cl]Cl. The second-order rate constant at 298 K and $\mu = 0.5$ M is $k_H = 10 \times 10^{-2}$ M^{-1} s^{-1} and is nine orders of magnitude slower than that reported for the protonolysis of *cis*-$[Pt(PEt_3)_2(Me)_2]$ in methanol [30]. A detailed kinetic study of the protonolysis of $[Pt(N–N–N)(Me)]^+$ (N–N–N = substituted tpy and dien) complexes in water is currently underway and the results will be published elsewhere.

The reaction of [**1**]Cl with CO has been carried out in D_2O solution at room temperature. After 24 h reaction time, the ^{1}H-NMR analysis of the final equilibrium mixture showed the presence of a large amount of unreacted material and acetone as the only organic product. Unsoluble tpy and metallic platinum separated out from the solution. These results, together with the observation that diluted aqueous solution of [**1**]Cl appear to be completely unreactive toward carbonylation, leads to wonder to what extent platinum dimers can promote carbon monoxide uptake and offer a suitable site for the coupling of the organic fragments in the formation of acetone. Carbon monoxide adds to [Pt(N–N)(Me)Cl] (N–N = α,α′-diimine ligands) to afford neutral five-coordinate [Pt(N–N)(Me)(CO)Cl] or cationic four-coordinate $[Pt(N–N)(Me)(CO)]^+$, depending on the steric crowding of the *N*,*N*-ligand [31]. Carbonyl for chloride substitution occurs on carbonylation of cyclometallated [Pt(N–N–C)Cl] complexes [32].

In conclusion, the $[Pt(tpy)(Me)]^+$ cation in water shows a remarkable inertness toward nucleophilic and electrophilic attacks, and toward carbonyl insertion into the Pt–CH_3 bond. The role played in these reactions by oligomerization of the complex in water remain to be clarified.

3. Supplementary material

Fig. S1 showing the unit cell of compound [**1**](BPh_4) and tables giving complete crystallographic data, bond distances, bond angles, anisotropic thermal parameters, and hydrogen atom coordinates (19 pages).

Acknowledgements

The authors wish to thank Professor David R. McMillin for helpful suggestions, the Ministero dell' Universita' e della Ricerca Scientifica e Tecnologica (MURST), Programmi di Ricerca Scientifica di Rilevante Interesse Nazionale, Cofinanziamento 1998–1999, and CNR for funding this work.

References

[1] E.M.A. Ratilla, B.K. Scott, M.S. Moxness, N.M. Kostic, Inorg. Chem. 29 (1990) 918.

[2] E.M.A. Ratilla, N.M. Kostic, J. Am. Chem. Soc. 110 (1988) 4427.
[3] (a) S.J. Lippard, Acc. Chem. Res. 11 (1978) 211. (b) K.W. Jennette, J.T. Gill, J.A. Sadownick, S.J. Lippard, J. Am. Chem. Soc. 98 (1976) 6159.
[4] M.G. Hill, J.A. Bailey, V.M. Miskowski, H.B. Gray, Inorg. Chem. 35 (1996) 4585.
[5] J.A. Bailey, M.G. Hill, R.E. Marsh, V.M. Miskowski, W.P. Schaefer, H.B. Gray, Inorg. Chem. 34 (1995) 4591.
[6] A.W. Roszak, O. Clement, E. Buncel, Acta Crystallogr. Sect. C 52 (1996) 1645.
[7] J.A. Bailey, V.J. Catalano, H.B. Gray, Acta Crystallogr. Sect. C 49 (1993) 1598.
[8] M. Akiba, Y. Sasaki, Inorg. Chem. Commun. 1 (1998) 61.
[9] H.-K. Yip, L.-K. Cheng, K.-K. Cheung, C.-M. Che, J. Chem. Soc. Dalton Trans. (1993) 2933.
[10] T.K. Aldridge, E.M. Stacy, D.R. Mc Millin, Inorg. Chem. 33 (1994) 722.
[11] J.A. Bailey, V.M. Miskowski, H.B. Gray, Inorg. Chem. 32 (1993) 369.
[12] D.K. Crites, C.T. Cunningham, D.R. McMillin, Inorg. Chim. Acta 273 (1998) 346.
[13] G. Arena, L. Monsù Scolaro, R.F. Pasternack, R. Romeo, Inorg. Chem. 34 (1995) 2994.
[14] R. Romeo, L. Monsù Scolaro, Inorg. Synth. 32 (1998) 153.
[15] M. Casamento, G.E. Arena, C. Lo Passo, I. Pernice, A. Romeo, L. Monsù Scolaro, Inorg. Chim. Acta 275-6 (1998) 242.
[16] L. Monsù Scolaro, A. Romeo, A. Terracina, Chem. Commun. (Cambridge) (1997) 1451.
[17] G. Arena, G. Calogero, S. Campagna, L. Monsù Scolaro, V. Ricevuto, R. Romeo, Inorg. Chem. 37 (1998) 2763.
[18] C. Eaborn, K. Kundu, A.J. Pidcock, J. Chem. Soc. Dalton Trans. (1981) 933.
[19] The assignment follows the numeration pattern shown in Fig. 1.
[20] MOLEN Enraf-Nonius Structure Determination Package, Enraf-Nonius, Delft, The Netherlands, 1990.
[21] A.C.T. North, D.C. Phillips, F.S. Mathews, Acta Crystallogr. Sect. A 24 (1968) 351.
[22] International Tables for X-ray Crystallography; A.J.C. Wilson (Ed.), vol. C, Kluwer Academic, Dordrecht, The Netherlands, 1992.
[23] G.M. Sheldrick SHELX-97. Structure solution and refinement package. Universität Göttingen, Germany, 1997.
[24] Cambridge Structural Data Base (1992–1997). Cambridge Crystallographic Data Centre, 123 Union Road, Cambridge, UK.
[25] R.E. Rülke, V.E. Kaasjager, D. Kliphuis, C.J. Elsevier, P.W.N.M. van Leeuwen, K. Vrieze, K. Govbitz, Organometallics 15 (1996) 668.
[26] L. Cattalini, private communication.
[27] (a) L.J. Andrews, J. Phys. Chem. 83 (1979) 3203. (b) F. Barigelletti, D. Sandrini, M. Maestri, V. Balzani, A. von Zelewsky, L. Chassot, P. Jolliet, U. Maider, Inorg. Chem. 27 (1988) 3644.
[28] R. Bucher, J.S. Field, R.J. Haines, C.T. Cunningham, D.R. McMillin, Inorg. Chem. 36 (1997) 3952.
[29] B. Pitteri, G. Marangoni, L. Cattalini, T. Bobbo, J. Chem. Soc. Dalton Trans. (1995) 3853.
[30] R. Romeo, M.R. Plutino, L.I. Elding, Inorg. Chem. 36 (1997) 5909.
[31] V. De Felice, A. De Renzi, M.L. Ferrara, A. Panunzi, J. Organomet. Chem. 513 (1996) 97.
[32] M.A. Cinellu, A. Doppiu, G. Minghetti, S. Stoccoro, A. Zucca, Abstracts from the Meeting Principles and Applications of Metal-Assisted Reactions Parma, Italy, March 19th, 1999.